A study on the characteristics of externally pressurized air bearings

Dong-chul Han, Sang-shin Park, Woo-jung Kim, and Jong-won Kim
Department of Mechanical Design and Production Engineering, Seoul National University, Seoul, Korea

In this study the direct numerical method is applied to solve the perturbed Reynolds' equation. To solve it the perturbed dimensionless mass flow rate is used as the boundary condition under the inherently compensated restrictor. The dynamic characteristics of a rotor supported in the externally pressurized air bearings, such as stiffness and damping coefficients, are analyzed, and as a result the orbit of the journal center due to rotating unbalance force is calculated. The diameter of the orbit has been experimentally determined based on the three-point method. The maximum difference between the measured and calculated diameters was less than 5%.

Keywords: *air bearings; Reynolds' equation*

Introduction

The development of ultraprecision machining equipment plays an important role in the recent research activities in the area of electronics and optics. The spindle unit is one of the most important factors in determining the overall performance of an ultraprecision machine.

Air bearings are usually used as the main spindle bearings of the machine tools for small and light workpieces. Especially, the externally pressurized air bearings support relatively high load even at zero spin rate and are free from wear when accelerating and decelerating due to the air film generated by the externally compressed air. Compared with oil bearings, air bearings have less heat generation, low contamination, and high accuracy.

For the design of an accurate high-speed spindle with externally pressurized air bearings, the analysis of rotor-dynamic characteristics such as bearing stiffness and damping coefficients is very important, as is the analysis of static characteristics such as bearing load capacity and required air flow rate.

As a design guide, a well-known Mechanical Technology Inc. (MTI) gas bearing design manual[1,2] is available. Gross[3] also summarized some of the design details. However, these studies assumed a line source, which led to the insufficient description of the circular flow motion under the point sources such as the air supply restrictors.

Address reprint requests to Dong-chul Han, Department of Mechanical Design and Production Engineering, Seoul National University, San 56-1, Shilim-Dong, Kwanak-Ku, Seoul, Korea.

Hence, several analytical methods that adapted the point source assumption have been developed. Majumdar[4] proposed a method that used the influence coefficients between each air supply restrictor. Elrod et al.[5] and Kazimierski et al.[6] transformed the governing equation into a difference equation and substituted the influence of supply flow rate into the difference equation.

Recently, the direct numerical method has been recognized as very effective in solving the air bearing problem.[7] Kawabata[8] analyzed the air film for a high bearing number (high Λ) and compared the results with those by the finite element method. Park[9] established a direct numerical method considering the slip condition of the air particles on the bearing surface and compared the results with those obtained by an indirect method using $\Psi = P^2H^2$. However, the direct numerical methods mentioned above did not include external air supply sources.

Also, it is important to calculate the orbit of the rotor shaft center due to rotating unbalance force because the orbit affects the spinning accuracy of the spindle unit. To obtain the orbit of the rotor shaft center, the forces exerted from the air film, which are dependent on the stiffness and damping coefficients of the air bearing, should be calculated. Hunger[10] studied this subject and obtained the rotor-dynamic coefficients and air film forces for several types of air bearings. However, he did not present a strict analysis based on the orbit of the rotor shaft center.

In this article, a direct numerical method is extended to solve the governing equation, which includes the external air supply sources with a boundary condition based on the continuity properties of mass flow rate. Also, the nonlinear equations of

motion of the rotor-bearing systems are solved to obtain the orbit of the rotor shaft center, and the results of the theoretical analyses are compared with those of an experimental study.

In the following section, the governing equation is summarized and a direct numerical method and boundary conditions are presented to solve the equation. The analytical method to calculate the orbit of the rotor shaft center is addressed next, followed by an example of specific numerical design, where stiffness and damping coefficients of a given air bearing are analyzed. Finally, experimental results are shown and compared with the theoretical calculation of the orbit of the rotor shaft center.

Governing equation

The Reynolds' equation for a compressible fluid is presented as follows with the geometry based on *Figure 1*.

$$\frac{\partial}{\partial\theta}\left(PH^3\frac{\partial P}{\partial\theta}\right)+\frac{\partial}{\partial\zeta}\left(PH^3\frac{\partial P}{\partial\zeta}\right)=\Lambda\frac{\partial}{\partial\theta}(PH)+2\Lambda\frac{\partial}{\partial\tau}(PH) \tag{1}$$

It is assumed that F_{st} is exerted only along the y-axis in *Figure 2*, and the instant center of the rotor shaft is assumed to be moving in a relatively narrow range. Then the perturbed film thickness is

$$H = H_0 + H_1\cdot\Delta x + H_2\cdot\Delta y \tag{2}$$

where $H_1 = -\sin\theta$ and $H_2 = -\cos\theta$

The x and y components of shaft vibration are assumed to be harmonic and then the perturbed pressure term is expressed in a complex form:

$$P = P_0 + P_1\cdot\Delta x + P_2\cdot\Delta y \tag{3}$$

where $P_1 = P_1^0 + i\cdot P_1^*$ and $P_2 = P_2^0 + i\cdot P_2^*$.

Substituting Equations (2) and (3) into Equation (1) yields the following perturbed Reynolds' equation:

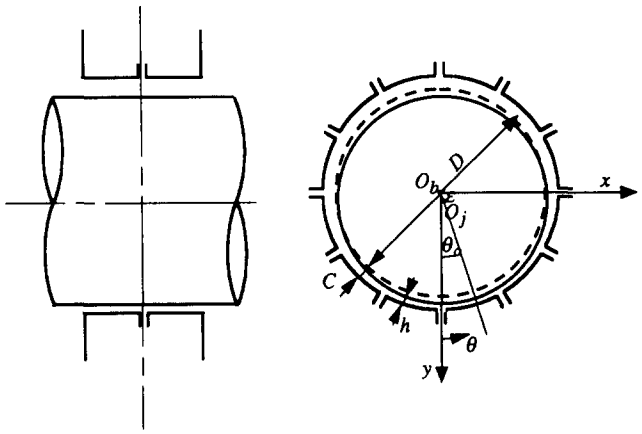

Figure 1 Schematics of the externally pressurized gas journal bearing

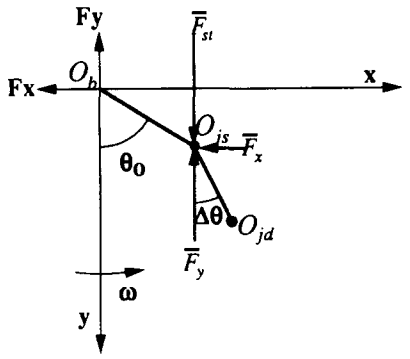

Figure 2 Coordinate system used in dynamic analysis

tion:

$$\frac{\partial}{\partial\theta}\left(P_0H_0^3\frac{\partial P_0}{\partial\theta}\right)+\frac{\partial}{\partial\zeta}\left(P_0H_0^3\frac{\partial P_0}{\partial\zeta}\right)=\Lambda\frac{\partial}{\partial\theta}(P_0H_0) \tag{4}$$

$$\frac{\partial}{\partial\theta}\left[P_0H_0^3\frac{\partial P_1}{\partial\theta}+3P_0H_0^2H_1\frac{\partial P_0}{\partial\theta}+H_0^3P_1\frac{\partial P_0}{\partial\theta}\right]+\frac{\partial}{\partial\zeta}\left[P_0H_0^3\frac{\partial P_1}{\partial\zeta}+3P_0H_0^2H_1\frac{\partial P_0}{\partial\zeta}+H_0^3P_1\frac{\partial P_0}{\partial\zeta}\right]=\Lambda\frac{\partial}{\partial\theta}(P_0H_1+P_1H_0)+2\Lambda i(P_0H_1+P_1H_0) \tag{5}$$

$$\frac{\partial}{\partial\theta}\left[P_0H_0^3\frac{\partial P_2}{\partial\theta}+3P_0H_0^2H_2\frac{\partial P_0}{\partial\theta}+H_0^3P_2\frac{\partial P_0}{\partial\theta}\right]+\frac{\partial}{\partial\zeta}\left[P_0H_0^3\frac{\partial P_2}{\partial\zeta}+3P_0H_0^2H_2\frac{\partial P_0}{\partial\zeta}+H_0^3P_2\frac{\partial P_0}{\partial\zeta}\right]=\Lambda\frac{\partial}{\partial\theta}(P_0H_2+P_2H_0)+2\Lambda i(P_0H_2+P_2H_0) \tag{6}$$

Because the solution to Equation (4) is suggested by Jeon et al.,[11] the direct numerical method to solve perturbed differential Equations (5) and (6) is discussed in this article.

Transforming Equations (5) and (6) into vector forms gives the following equation:

$$\nabla\cdot[P_0H_0^3\nabla P_k+3P_0H_0^2H_k\nabla P_0+H_0^3P_k\nabla P_0-\underline{\Lambda}(P_0H_k+P_kH_0)]=2\Lambda i(P_0H_k+P_kH_0) \tag{7}$$

where $k = 1, 2$. Integrating Equation (7) along the lubricated surface $\Sigma_{i,j}$, which encompasses the arbitrary point (i, j) in *Figure 3* yields

$$\iint_{\sum_{ij}}\nabla\cdot[P_0H_0^3\nabla P_k+3P_0H_0^2H_k\nabla P_0+H_0^3P_k\nabla P_0-\underline{\Lambda}(P_0H_k+P_kH_0)]\,d\theta\cdot d\zeta=\iint_{\sum_{ij}}2\Lambda i(P_0H_k+P_kH_0)\,d\theta\cdot d\zeta \tag{8}$$

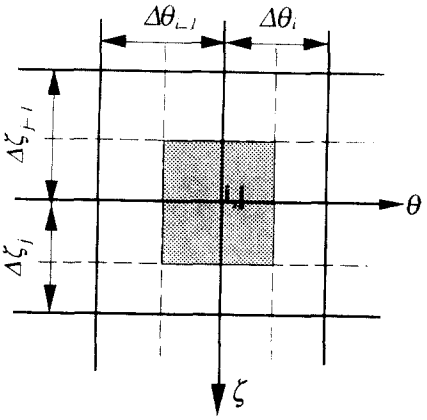

Figure 3 Mesh defined for analysis

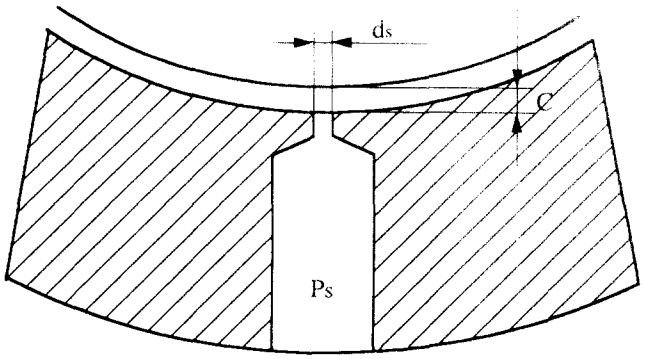

Figure 4 Schematics of an inherent compensated air supply restrictor

Then, Gauss' divergence theorem is applied to obtain the following result:

$$\oint_{\Gamma_i} [P_0 H_0^3 \nabla P_k + 3P_0 H_0^2 H_k \nabla P_0 + H_0^3 P_2 \nabla P_0 - \underline{\Lambda}(P_0 H_k + P_k H_0)] \underline{n} \cdot dl = \iint_{\sum_i} 2\Lambda i (P_0 H_k + P_k H_0)\, d\theta \cdot d\zeta \quad (9)$$

If the functions of pressure and clearance are assumed to be linear in the control surface shown in *Figure 3*, then, by using a central difference equation, the following simple algebraic equation is obtained for each mesh point from Equation (9):

$$A_{ki,j}P_{ki,j} = A_{ki-1,j}P_{ki-1,j} + A_{ki+1,j}P_{ki+1,j} + A_{ki,j-1}P_{ki,j-1} + A_{ki,j+1}P_{ki,j+1} + A_{dk} - I_k \quad (10)$$

where each coefficient is listed in Appendix A.

At the mesh points located on the air supply restrictors, the continuity condition for mass flow rate is used. The dimensionless mass flow rate through the inherent compensated air supply restrictor shown in *Figure 4* is obtained assuming the isotropic process for compressible fluid[12]:

$$Q_s = \Gamma_s P_s H \Phi \quad (11)$$

where Φ is expressed as follows:

$$\Phi = \left[\frac{2\kappa}{\kappa+1}\right]^{1/2}\left[\frac{2}{\kappa+1}\right]^{1/(\kappa-1)}, \quad \frac{p_{ij}}{p_s} \le \left[\frac{2}{\kappa+1}\right]^{\kappa/(\kappa-1)} \quad (12)$$

or

$$\Phi = \left[\frac{2\kappa}{\kappa-1}\right]^{1/2}\left[\left(\frac{p_{ij}}{p_s}\right)^{2/\kappa} - \left(\frac{p_{ij}}{p_s}\right)^{(\kappa+1)/\kappa}\right]^{1/2}, \quad \frac{p_{ij}}{p_s} > \left[\frac{2}{\kappa+1}\right]^{\kappa/(\kappa-1)} \quad (13)$$

The perturbed flow rate equation for the control surface that has a feeding hole can be obtained by substituting Equations (2) and (3) into Equation (11) as follows:

$$Q_s = Q_0 + Q_1 \Delta x + Q_2 \Delta y \quad (14)$$

where Q_1 and Q_2 are listed in Appendix B.

This flow rate variation is added to algebraic Equation (10) at each mesh point located on the air supply restrictor:

$$A_{ki,j}P_{ki,j} = A_{ki-1,j}P_{ki-1,j} + A_{ki+1,j}P_{ki+1,j} + A_{ki,j-1}P_{ki,j-1} + A_{ki,j+1}P_{ki,j+1} + A_{dk} - I_k + Q_k \quad (15)$$

The boundary conditions for Equations (10) and (15) are as follows:

1. At each boundary of bearing: $P_0 = 1$, $P_k = 0$.
2. Periodicity: $P_0(\theta) = P_0(2\pi + \theta)$, $P_k(\theta) = P_k(2\pi + \theta)$.

By solving Equations (10) and (15), the perturbed pressure P_1 and P_2 are obtained, and the stiffness and damping coefficients are calculated by integrating P_1 and P_2 along bearing width and each coordinate:

$$\gamma_{11} = \frac{K_{11}\cdot C}{p_a \cdot B \cdot D} = \frac{1}{4 \cdot D/B}\int_0^{2\pi}\int_0^{B/R} \mathrm{Re}(P_1)\cdot\sin(\theta)\, d\zeta\, d\theta$$

$$\gamma_{12} = \frac{K_{12}\cdot C}{p_a \cdot B \cdot D} = \frac{1}{4 \cdot D/B}\int_0^{2\pi}\int_0^{B/R} \mathrm{Re}(P_2)\cdot\sin(\theta)\, d\zeta\, d\theta$$

$$\gamma_{21} = \frac{K_{21}\cdot C}{p_a \cdot B \cdot D} = \frac{1}{4 \cdot D/B}\int_0^{2\pi}\int_0^{B/R} \mathrm{Re}(P_1)\cdot\cos(\theta)\, d\zeta\, d\theta$$

$$\gamma_{22} = \frac{K_{22} \cdot C}{p_a \cdot B \cdot D} = \frac{1}{4 \cdot D/B} \int_0^{2\pi} \int_0^{B/R} \mathrm{Re}(P_2) \cdot \cos(\theta)\, d\zeta\, d\theta$$

$$\beta_{11} = \frac{D_{11} \cdot C \cdot \omega}{p_a \cdot B \cdot D} = \frac{1}{4 \cdot D/B} \int_0^{2\pi} \int_0^{B/R} \mathrm{Im}(P_1) \cdot \sin(\theta)\, d\zeta\, d\theta$$

$$\beta_{12} = \frac{D_{12} \cdot C \cdot \omega}{p_a \cdot B \cdot D} = \frac{1}{4 \cdot D/B} \int_0^{2\pi} \int_0^{B/R} \mathrm{Im}(P_2) \cdot \sin(\theta)\, d\zeta\, d\theta$$

$$\beta_{21} = \frac{D_{21} \cdot C \cdot \omega}{p_a \cdot B \cdot D} = \frac{1}{4 \cdot D/B} \int_0^{2\pi} \int_0^{B/R} \mathrm{Im}(P_1) \cdot \cos(\theta)\, d\zeta\, d\theta$$

$$\beta_{22} = \frac{D_{22} \cdot C \cdot \omega}{p_a \cdot B \cdot D} = \frac{1}{4 \cdot D/B} \int_0^{2\pi} \int_0^{B/R} \mathrm{Im}(P_2) \cdot \cos(\theta)\, d\zeta\, d\theta$$

The forces exerted from air film are then obtained:

$$\bar{F}_x = 0 + \gamma_{11}(\varepsilon, \theta) \cdot \Delta x + \gamma_{12}(\varepsilon, \theta) \cdot \Delta y + \beta_{11}(\varepsilon, \theta) \cdot \Delta \dot{x} + \beta_{12}(\varepsilon, \theta) \cdot \Delta \dot{y} \quad (16)$$

$$\bar{F}_y = \bar{F}_{st} + \gamma_{21}(\varepsilon, \theta) \cdot \Delta x + \gamma_{22}(\varepsilon, \theta) \cdot \Delta y + \beta_{21}(\varepsilon, \theta) \cdot \Delta \dot{x} + \beta_{22}(\varepsilon, \theta) \cdot \Delta \dot{y} \quad (17)$$

where $\Delta x = \varepsilon \sin\theta - \varepsilon_0 \sin\theta_0$, $\Delta y = \varepsilon \cos\theta - \varepsilon_0 \cos\theta_0$.

Orbit calculation due to rotating unbalance force

In the coordinate system shown in *Figure 5*, O_{js} is the steady-state position of the rotor shaft center around which O_{jd} spins with the unbalance of 0.5 $m_w e_\rho$. The nonlinear equation of motion of the rigid rotor-bearing system is as follows, where all the variables are in dimensionless forms:

$$\bar{F}_{st}\left(\frac{\omega}{\omega_0}\right)^2 [\ddot{\varepsilon} - \varepsilon\dot{\theta}^2] = -\bar{F}_\varepsilon + \bar{F}_{st}\cos\theta + \bar{F}_{st}\left(\frac{\omega}{\omega_0}\right)^2 \varepsilon_\rho \cos(\tau - \theta) \quad (18)$$

$$\bar{F}_{st}\left(\frac{\omega}{\omega_0}\right)^2 [\varepsilon\ddot{\theta} + 2\dot{\varepsilon}\dot{\theta}] = -\bar{F}_\theta - \bar{F}_{st}\cos\theta + \bar{F}_{st}\left(\frac{\omega}{\omega_0}\right)^2 \varepsilon_\rho \sin(\tau - \theta) \quad (19)$$

where $\varepsilon = e/C$, $\varepsilon_\rho = e_\rho/C$, $\bar{F}_{st} = m_w g/2p_a BD$, $\omega_0^2 = g/C$

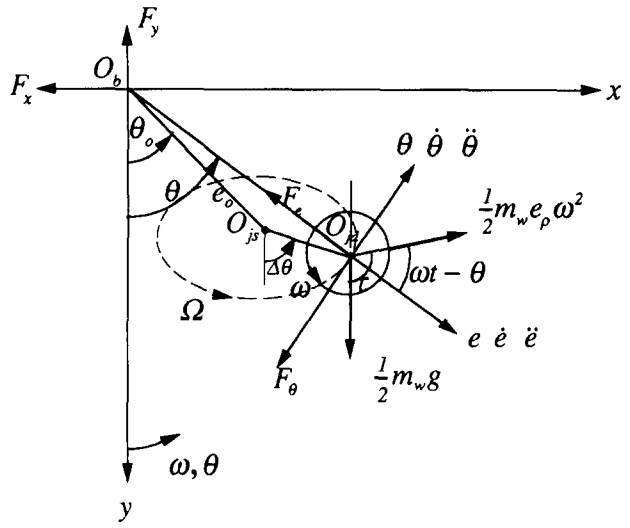

Figure 5 Coordinate system for nonlinear equation of rigid rotor motion

and bearing forces $\bar{F}_\varepsilon$ *and* $\bar{F}_\theta$ *are*

$$\bar{F}_\varepsilon = \bar{F}_x \cdot \sin\theta + \bar{F}_y \cdot \cos\theta \quad (20)$$

$$\bar{F}_\theta = \bar{F}_x \cdot \cos\theta - \bar{F}_y \cdot \sin\theta \quad (21)$$

Equations (18) and (19) can be solved applying the Runge-Kutta method with initial conditions for ε_0 and θ_0 obtained at each static equilibrium point, and those for $\dot{\varepsilon}_0$ and $\dot{\theta}_0$ assumed to be zero. The dimensionless time interval $\Delta\tau$ is 0.001.

Specific design analysis

The theoretical analysis method presented in previous sections is applied to an air bearing with its major dimensions $B/D = 38/60$ and C = 10 μm. The supply restrictors are assumed to be equally spaced along the circumference. The mesh for the difference equation is generated by dividing the circumferential and axial lengths by 60 and 16, respectively. The convergence limits for steady-state and perturbed pressure distributions are, respectively,

$$\max|P_{oij}^{(v)} - P_{oij}^{(v-1)}| < 10^{-7}$$

and

$$\max|P_{kij}^{(v)} - P_{kij}^{(v-1)}| < 10^{-5}.$$

Figure 6 shows the comparison between the dimensionless static stiffness coefficient $\bar{F}/\varepsilon$ and the dimensionless rotor-dynamic stiffness coefficient obtained by the analysis used in this study when $\Lambda = 1$ and $\varepsilon = 0.1$ with the supply pressures of 0.5 and 0.7 MPa. The solid and dotted lines in *Figure 6* present dynamic and static stiffness, respectively. Both stiffness coefficients coincide as the feeding parameter increases over 0.6.

The principal stiffness and damping coefficients γ_{11} and β_{11}, are shown in *Figure 7*. In this case, the

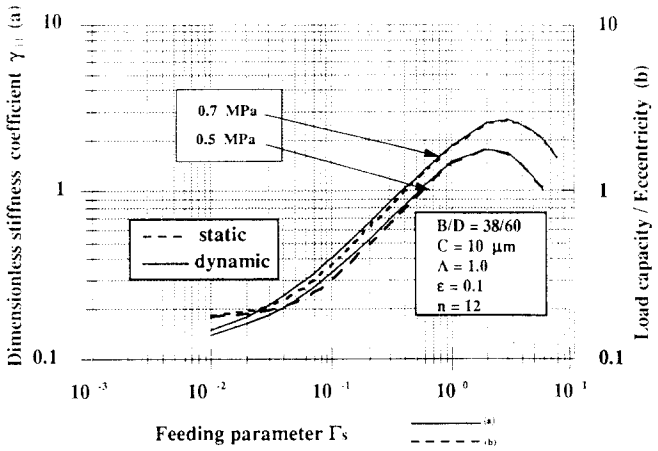

Figure 6 Comparison of static stiffness between dynamic stiffness coefficients

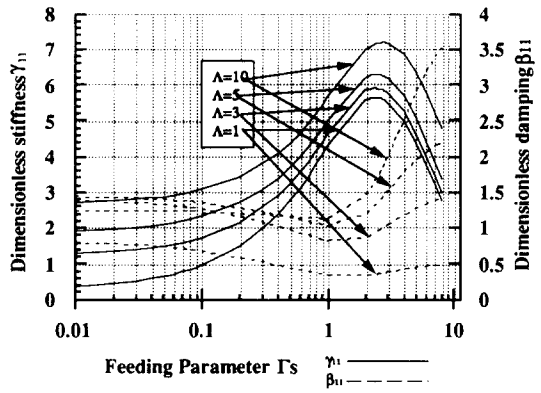

Figure 7 Feeding parameter versus stiffness and damping coefficients (Ps = 6)

supply pressure is 0.6 MPa and the eccentricity ratio is 0.1. A set of design parameters exist that yield a maximum stiffness for a given supply pressure. However, the damping coefficient reaches its minimum value with this set of design parameters.

Figure 8 shows the stiffness coefficients γ_{11} and the damping coefficients β_{11} for various *B/D* ratios at the same condition as in *Figure 7*. The stiffness coefficients and damping coefficients increase as the *B/D* ratio increases. But the value of the feeding parameter which yields maximum stiffness decreases slightly as the *B/D* ratio increases.

Figure 9 presents the stiffness coefficients γ_{11} according to the number of air supply restrictors. The supply pressure is 0.6 MPa ($\Lambda = 1$ and $\varepsilon = 0.1$). As the number of air supply restrictors increases, the stiffness coefficient gets higher. However, the differences between maximum stiffnesses are within 10% when the number of restrictors is more than eight.

The stiffness coefficients also increase as the supply pressure is increased, as shown in *Figure 10*. In this case, compressibility is 1.0, the eccentricity ratio is 0.1, and the number of restrictors is 12. The maximum stiffness coefficients are linearly proportional to the supply pressure.

Figures 11 and *12* show the stiffness and damping coefficients, respectively, versus the eccentricity ε. In this case, compressibility is 1.0, the feeding parameter is 2.4 and the attitude angle is 0. If ε is relatively small, the two principal coefficients are almost the same and the two coupled coefficients

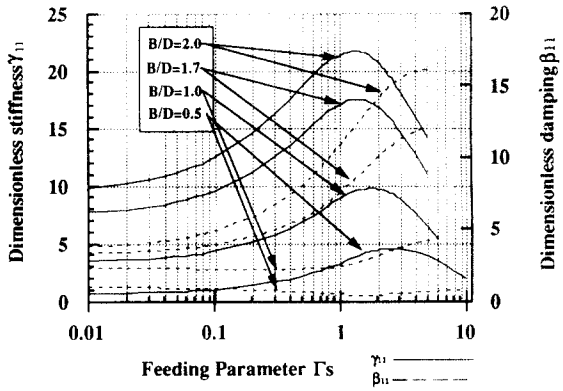

Figure 8 Influence of B/D ratio

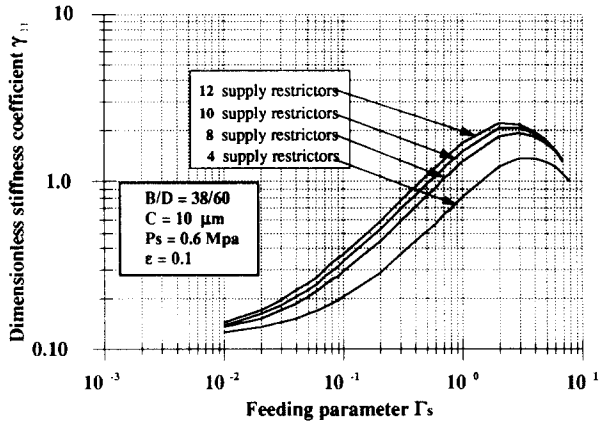

Figure 9 Influence of number of supply restrictors ($\Lambda = 1$, Ps = 6)

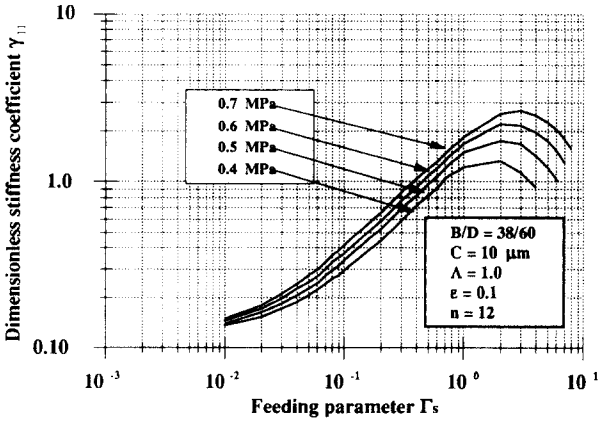

Figure 10 Influence of supply pressure ($\Lambda = 1$, n = 12)

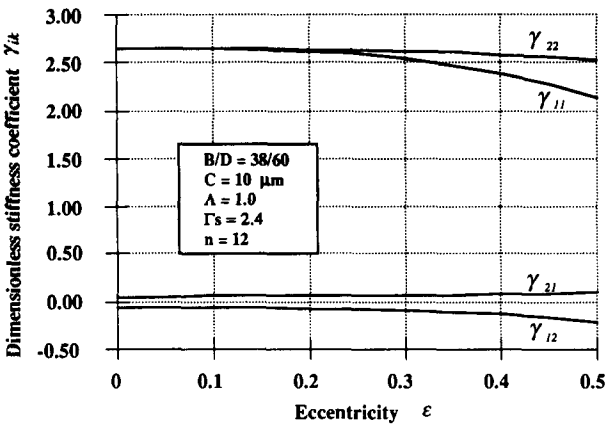

Figure 11 Stiffness coefficients versus eccentricity ($\Lambda = 1$)

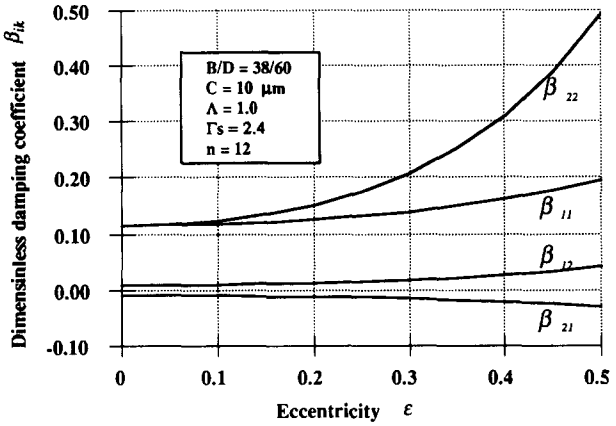

Figure 12 Damping coefficients versus eccentricity ($\Lambda = 1$)

have the same magnitude with reversed signs. The stiffness γ_{12} and damping β_{21} have negative values. This finding coincides with other results of general journal-bearing characteristics. Also, it is the magnitude of the coupled coefficients relative to the principal coefficients that influences stability of a rotor-bearing system. Because in our model the absolute values of the coupled stiffness and damping are small compared with the principal stiffness and damping, there is no need to consider stability here.

As ε increases, γ_{22} becomes larger than γ_{11} because the eccentricity is in the y direction only. In the case of damping coefficients, β_{22} increases rapidly as ε becomes larger due to the squeeze effect.

Experimental study

This section describes the comparison between the theoretical calculation and the experimental results of the orbit of the rotor shaft center. In general, the orbit of a rigid rotor-bearing system supported by an air bearing is smaller than the geometrical error including roundness. For this reason, the three-point measuring method[13] is used to measure the accuracy of the spindle rotation.

Figure 13 is a schematic diagram of the experimental set-up. The field balancing of the spindle is performed according to the procedure proposed by Ozawa[14] to eliminate the effect of unbalance. Three capacitance-type PDG-210 gap sensors are attached to each end of the bearing supports and the gains are adjusted so that all three sensors have the same gain value of 1.5748 V/μm. Initially, the balancing of the spindle is set to be within 0.1 g at the radial distance of 38.1 mm with 2,000 rpm.

Figures 14 and *15* show the calculated orbits (solid lines) of the rotor shaft center compared with

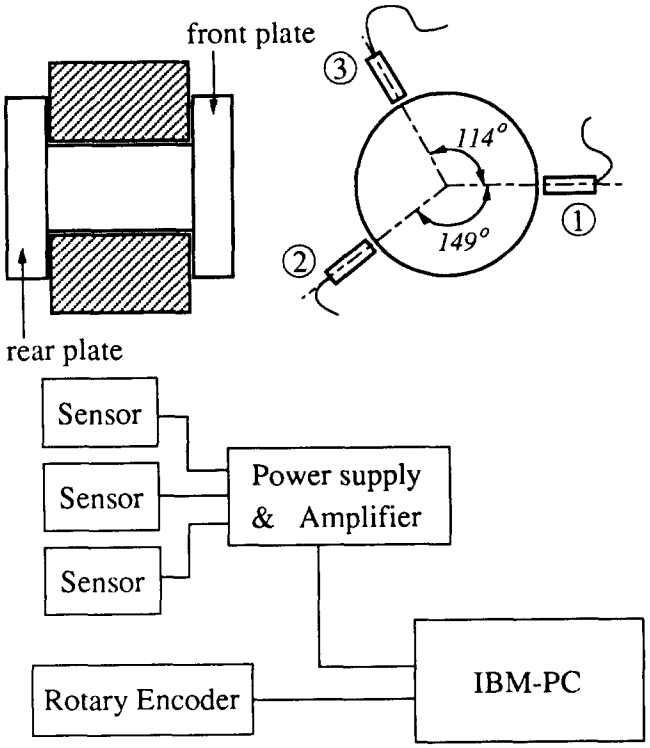

Figure 13 Schematic diagram of experimental set-up

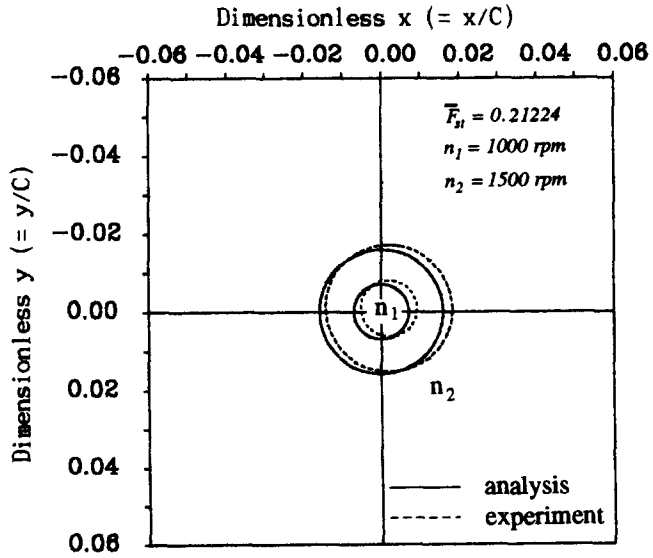

Figure 14 Dimensionless orbit of rotor shaft center

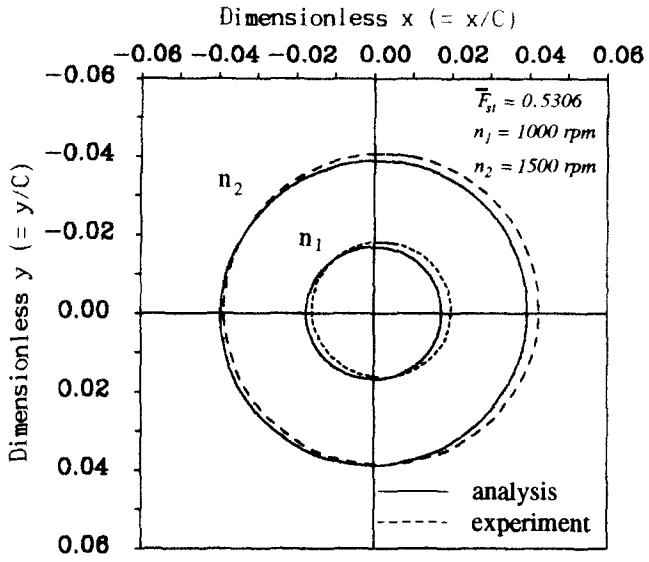

Figure 15 Dimensionless orbit of rotor shaft center

the measured orbits (dotted lines). The orbits are shown in *Figure 14* for two different rpm. When F_{st} is 0.21224, the clearance is 10 μm, and the diameter of the supply restrictors is 0.25 mm. *Figure 15* shows that the diameters of the orbits are increased as the unbalance increases ($F_{st} = 0.5306$).

At 1,000 rpm, the maximum diameters of the calculated and measured orbits are 0.0141 and 0.01481 as shown in *Figure 14*. The difference between the orbits from the analytical analysis and experimental study is less than 5%. This difference may be due to roundness of the air bearing, which is about 2 μm. Thus, the accurate orbit of a shaft supported on externally pressurized air bearings due to rotating unbalance force can be predicted at the design stage.

Conclusion

The static and dynamic characteristics such as stiffness and damping coefficients has been calculated by using a direct numerical method to solve the perturbed Reynolds' equation. There exists a feeding coefficient Γ_S to yield a maximum stiffness coefficient and a minimum damping coefficient. The stiffness coefficient changes rapidly with the variation of feeding coefficients Γ_S; however, it is insensitive to the compressibility coefficient Λ. The damping coefficient showed an opposite trend compared with the stiffness coefficient: a gradual change with feeding parameter Γ_S, but sensitive to the compressibility coefficient Λ. This is because the squeeze effect increases as the spinning speed increases, which influences the damping coefficients.

The orbit of the rotor shaft center can be obtained by solving the nonlinear equation of motion of the rigid rotor-bearing system. The diameter of the orbit has been experimentally determined based on the three-point method. The maximum difference between the measured and calculated diameters was less than 5%.

References

1 Reiger, N. F., ed. "Design of gas bearings." RPI-MTI Gas Bearing Design Course, Latham, NY: Mechanical Technology Inc., 1967
2 Wilcock, D. F., ed. *MTI Gas Bearing Design Manual*, Latham, NY: Mechanical Technology Inc., 1972
3 Gross, W. A. *Fluid Film Lubrication*. New York: Wiley, 1980
4 Majumdar, B. C. "On the general solution of externally pressurized gas journal bearings," *J Lub Tech Trans ASME* 1972, **94**, 291–296
5 Elrod, H. G. and Glanfield, G. A. "Computer procedures for the design of flexibly mounted, externally pressurized, gas lubricated journal bearings," Proceedings of 5th Gas Bearing Symposium, University of Southampton, paper 22, 1971
6 Kazimierski, Z. and Trojnarski, J. "Investigations of externally pressurized gas bearings with different feeding systems," *J Lub Tech Trans ASME* 1980, **103**, 59–64
7 Castelli, V. and Pirvics, J. "Review of numerical methods in gas bearing film analysis," *J Lub Tech Trans ASME* 1968, **90**, 777–792
8 Kawabata, N. "Numerical analysis of Reynolds equation for gas lubrication in a high Λ region," *JSME Int J* 1987, **30**, 836–842
9 Sang-Shin Park, Pyung Hwang, In-Bae Chang, Dong-Chul Han. "Static analysis of gas bearing with ultra low clearance by the direct numerical solution method," *J KSME* 1991, **15**, 120–126 (in Korean)
10 Hunger, H. "Berechnung der statischen und dynamischen Kennlinien aerodynamische Ferderlager," Dissertation, University Karlsruhe, Karlsruhe, Germany, 1982
11 Kyung-suk Jeon, Dong-Chul Han, "Static and dynamic characteristics of aerostatic gas bearing," *J KSLE* 1990, **6**, 60–67 (in Korean)
12 Shapiro, A. H. *The Dynamics and the Thermodynamics of Compressibility Fluid Flow*. Vol. 1. New York: Ronald Press, 1953
13 Norimitsu Ozawa, Akinori Yui, Kimiyuki Mitsui. "Precision balancing of grinding wheels," *J JSPE* 1987, **53**, 140–145 (in Japanese)
14 Kimiyuki Mitsui. "A study on diagnosis technology of run-out accuracy of spindles—development of 3 point measuring method," *J JSME (C)* 1983, **48**, 115–123

Nomenclature

A_0	Reference curtain area of an inherent restrictor ($=\pi d_s C$)
B	Width of bearing
C	Clearance
C_d	Discharge coefficient
d_s	Diameter of the supply restrictor
dl	Infinitesimal length of grid contour
D	Diameter of bearing
D_{ij}	Damping coefficients
e	Eccentricity
e_0	Eccentricity at steady state
e_p	Radial distance of unbalance
F_{st}	Static load
$\bar{F}_{st}$	Dimensionless static load
F_x	x-component of resultant of pressure
$\bar{F}_x$	Dimensionless x-component of resultant of pressure
F_y	y-component of resultant of pressure
$\bar{F}_y$	Dimensionless y-component of resultant of pressure
$\bar{F}_r$	Dimensionless radial component of resultant of pressure

$\bar{F}_\theta$	Dimensionless circumferential component of resultant of pressure
g	Gravity acceleration
h	Film thickness function
H	Dimensionless film thickness function ($= h/C$)
H_0	Dimensionless film thickness at steady state ($= h_0/C$)
$H_{1,2}$ or H_k	Perturbed film thickness ($k = 1,2$)
K_{ij}	Stiffness coefficients
m_w	Mass of shaft
n	Number of the supply restrictors
$\underline{n}$	Unit normal vector
O_b	Bearing center
O_{jd}	Disturbed journal center
O_{js}	Journal center at static equilibrium state
p	Film pressure
p_a	Ambient pressure
p_s	Supply pressure
P	Dimensionless film pressure ($= p/p_a$)
P_0	Dimensionless film pressure at steady state ($= p_0/p_a$)
$P_{1,2}$ or P_k	Perturbed dimensionless film pressure ($= p_{1,2}/p_a$), ($k = 1,2$)
P_s	Dimensionless supply pressure ($= p_s/p_a$)
q_s	Mass flow rate supplied through the supply restrictor
Q_s	Dimensionless mass flow rate supplied through the supply restrictor
$Q_{1,2}$	Perturbed dimensionless mass flow rate supplied through the supply restrictor
r	Radius of bearing
$\boldsymbol{R}$	Gas constant
t	time
T	Temperature of supplied gas
β_{ij}	Dimensionless damping coefficients ($i = 1, 2, j = 1, 2$)
γ_{ij}	Dimensionless stiffness coefficients ($i = 1, 2, j = 1, 2$)
Γ_{ij}	Contour of control surface
Γ_s	Feeding parameter $\left(= \dfrac{12\mu C_d A_0 \sqrt{RT}}{p_a C^3}\right)$
ε	eccentricity ratio ($= e/C$)
ε_ρ	Dimensionless radial distance of unbalance
Φ	Orifice function
κ	Adiabatic number
Λ	Compressibility number $\left(= \dfrac{6\mu\omega r^2}{p_a C^2}\right)$
$\underline{\Lambda}$	Vector of compressibility number ($\underline{\Lambda} = \Lambda i$)
μ	Viscosity of gas
ν	Iteration number
θ	Circumferential coordinate
θ_0	Attitude angle at steady state
$\Delta\theta$	Circumferential coordinate of the disturbed position
Σ_{ij}	Area of control surface
ζ	Axial coordinate
τ	Dimensionless time
ω	Angular velocity of journal
ω_0	Reference angular velocity ($\omega_0^2 = g/C$)
Ω	Angular velocity of whirl

Appendix A

$$A_{k_{i-1,j}} = \left(-\frac{H^3_{0_{i-1/2,j+}}(P_{0_{i,j}} - P_{0_{i-1,j}})}{2\Delta\theta_i} + \frac{H^3_{0_{i-1/2,j+}} P_{0_{i-1/2,j}}}{\Delta\theta_i} + \frac{\Lambda H_{0_{i-1/2,j+}}}{2} \right) \cdot \frac{\Delta\zeta_{j+1}}{2}$$
$$+ \left(-\frac{H^3_{0_{i-1/2,j-}}(P_{0_{i,j}} - P_{0_{i-1,j}})}{2\Delta\theta_i} + \frac{H^3_{0_{i-1/2,j-}} P_{0_{i-1/2,j}}}{\Delta\theta_i} + \frac{\Lambda H_{0_{i-1/2,j+}}}{2} \right) \cdot \frac{\Delta\zeta_j}{2}$$

$$A_{k_{i+1,j}} = \left(+\frac{H^3_{0_{i+1/2,j+}}(P_{0_{i+1,j}} - P_{0_{i,j}})}{2\Delta\theta_{i+1}} + \frac{H^3_{0_{i+1/2,j+}} P_{0_{i+1/2,j}}}{\Delta\theta_{i+1}} - \frac{\Lambda H_{0_{i+1/2,j+}}}{2} \right) \cdot \frac{\Delta\zeta_{j+1}}{2}$$
$$+ \left(+\frac{H^3_{0_{i-1/2,j-}}(P_{0_{i+1,j}} - P_{0_{i,j}})}{2\Delta\theta_{i+1}} + \frac{H^3_{0_{i+1/2,j-}} P_{0_{i+1/2,j}}}{\Delta\theta_{i+1}} - \frac{\Lambda H_{0_{i+1/2,j-}}}{2} \right) \cdot \frac{\Delta\zeta_j}{2}$$

$$A_{k_{i,j-1}} = \left(-\frac{H^3_{0_{i+,j-1/2}}(P_{0_{i,j}} - P_{0_{i,j-1}})}{2\Delta\zeta_j} + \frac{H^3_{0_{i+,j-1/2}} P_{0_{i,i-1/2}}}{\Delta\zeta_j} \right) \cdot \frac{\Delta\theta_{i+1}}{2}$$
$$+ \left(-\frac{H^3_{0_{i-,j-1/2}}(P_{0_{i,j}} - P_{0_{i,j-1}})}{2\Delta\zeta_j} + \frac{H^3_{0_{i-,j-1/2}} P_{0_{i,i-1/2}}}{\Delta\zeta_j} \right) \cdot \frac{\Delta\theta_i}{2}$$

$$A_{k_{i,j+1}} = \left(\frac{H^3_{0_{i+,j+1/2}}(P_{0_{i,j+1}} - P_{0_{i,j}})}{2\Delta\zeta_{j+1}} + \frac{H^3_{0_{i+,j+1/2}} P_{0_{i,i-1/2}}}{\Delta\zeta_{j+1}} \right) \cdot \frac{\Delta\theta_{i+1}}{2} + \left(\frac{H^3_{0_{i-,j+1/2}}(P_{0_{i,j+1}} - P_{0_{i,j}})}{2\Delta\zeta_{j+1}} + \frac{H^3_{0_{i-,j+1/2}} P_{0_{i,i-1/2}}}{\Delta\zeta_{j+1}} \right) \cdot \frac{\Delta\theta_i}{2}$$

$$
\begin{aligned}
Ad_k = &\left(-3H^2_{0_{i,\,i-1/2,j}} H_{k_{i,\,i-1/2,j}} P_{0_{i-1/2,j}} \frac{P_{0_{i,j}} - P_{0_{i-1,j}}}{\Delta\theta_i} + \Lambda P_{0_{i-1/2,j}} H_{k_{i-1/2,j}} \right) \cdot \frac{\Delta\zeta_{j+1}}{2} \\
&+ \left(-3H^2_{0_{i-1/2,j-}} H_{k_{i-1/2,j}} P_{0_{i-1/2,j}} \frac{P_{0_{i,j}} - P_{0_{i-1,j}}}{\Delta\theta_i} + \Lambda P_{0_{i-1/2,j}} H_{k_{i-1/2,j}} \right) \cdot \frac{\Delta\zeta_j}{2} \\
&+ \left(3H^2_{0_{i+1/2,j+}} H_{k_{i+1/2,j}} P_{0_{i+1/2,j}} \frac{P_{0_{i+1,j}} - P_{0_{i,j}}}{\Delta\theta_{i+1}} - \Lambda P_{0_{i+1/2,j}} H_{k_{i+1/2,j}} \right) \cdot \frac{\Delta\zeta_{j+1}}{2} \\
&+ \left(3H^2_{0_{i+1/2,j-}} H_{k_{i+1/2,j}} P_{0_{i+1/2,j}} \frac{P_{0_{i+1,j}} - P_{0_{i,j}}}{\Delta\theta_{i+1}} - \Lambda P_{0_{i+1/2,j}} H_{k_{i+1/2,j}} \right) \cdot \frac{\Delta\zeta_j}{2} \\
&+ \left(-3H^2_{0_{i,j-1/2}} H_{k_{i,j-1/2}} P_{0_{i,j-1/2}} \frac{P_{0_{i,j}} - P_{0_{i,j-1}}}{\Delta\zeta_j} \right) \cdot \frac{\Delta\theta_{i+1}}{2} \\
&+ \left(-3H^2_{0_{i,j-1/2}} H_{k_{i,j-1/2}} P_{0_{i,j-1/2}} \frac{P_{0_{i,j}} - P_{0_{i,j-1}}}{\Delta\zeta_j} \right) \cdot \frac{\Delta\theta_i}{2} \\
&+ \left(3H^2_{0_{i,j+1/2}} H_{k_{i,j+1/2}} P_{0_{i,j+1/2}} \frac{P_{0_{i,j+1}} - P_{0_{i,j}}}{\Delta\zeta_j} \right) \cdot \frac{\Delta\theta_{i+1}}{2} \\
&+ \left(3H^2_{0_{i,j+1/2}} H_{k_{i,j+1/2}} P_{0_{i,j+1/2}} \frac{P_{0_{i,j+1}} - P_{0_{i,j}}}{\Delta\zeta_j} \right) \cdot \frac{\Delta\theta_i}{2}
\end{aligned}
$$

$$
\begin{aligned}
A_{k_{i,j}} = &\left(\frac{H^3_{0_{i-1/2,j+}} (P_{0_{i,j}} - P_{0_{i-1,j}})}{2\Delta\theta_i} + \frac{H^3_{0_{i-1/2,j+}} P_{0_{i-1/2,j}}}{\Delta\theta_i} - \frac{\Lambda H_{0_{i-1/2,j+}}}{2} \right) \cdot \frac{\Delta\zeta_{j+1}}{2} \\
&+ \left(\frac{H^3_{0_{i-1/2,j-}} (P_{0_{i,j}} - P_{0_{i-1,j}})}{2\Delta\theta_i} + \frac{H^3_{0_{i-1/2,j-}} P_{0_{i-1/2,j}}}{\Delta\theta_i} - \frac{\Lambda H_{0_{i-1/2,j+}}}{2} \right) \cdot \frac{\Delta\zeta_j}{2} \\
&+ \left(-\frac{H^3_{0_{i+1/2,j+}} (P_{0_{i+1,j}} - P_{0_{i,j}})}{2\Delta\theta_{i+1}} + \frac{H^3_{0_{i+1/2,j+}} P_{0_{i+1/2,j}}}{\Delta\theta_{i+1}} + \frac{\Lambda H_{0_{i+1/2,j+}}}{2} \right) \cdot \frac{\Delta\zeta_{j+1}}{2} \\
&+ \left(-\frac{H^3_{0_{i+1/2,j-}} (P_{0_{i+1,j}} - P_{0_{i,j}})}{2\Delta\theta_{i+1}} + \frac{H^3_{0_{i+1/2,j-}} P_{0_{i+1/2,j}}}{\Delta\theta_{i+1}} + \frac{\Lambda H_{0_{i+1/2,j-}}}{2} \right) \cdot \frac{\Delta\zeta_j}{2} \\
&+ \left(\frac{H^3_{0_{i,j-1/2}} (P_{0_{i,j}} - P_{0_{i,j-1}})}{2\Delta\zeta_j} + \frac{H^3_{0_{i,j-1/2}} P_{0_{i,i-1/2}}}{\Delta\zeta_j} \right) \cdot \frac{\Delta\theta_{i+1}}{2} \\
&+ \left(\frac{H^3_{0_{i-,j-1/2}} (P_{0_{i,j}} - P_{0_{i,j-1}})}{2\Delta\zeta_j} + \frac{H^3_{0_{i-,j-1/2}} P_{0_{i,i-1/2}}}{\Delta\zeta_j} \right) \cdot \frac{\Delta\theta_i}{2} \\
&+ \left(-\frac{H^3_{0_{i,j+1/2}} (P_{0_{i,j+1}} - P_{0_{i,j}})}{2\Delta\zeta_{j+1}} + \frac{H^3_{0_{i+,j+1/2}} P_{0_{i,i-1/2}}}{\Delta\zeta_{j+1}} \right) \cdot \frac{\Delta\theta_{i+1}}{2} \\
&+ \left(-\frac{H^3_{0_{i-,j+1/2}} (P_{0_{i,j+1}} - P_{0_{i,j}})}{2\Delta\zeta_{j+1}} + \frac{H^3_{0_{i-,j+1/2}} P_{0_{i,i-1/2}}}{\Delta\zeta_{j+1}} \right) \cdot \frac{\Delta\theta_i}{2}
\end{aligned}
$$

$$
I_k = \iint_{\sum_{i,j}} 2\Lambda i (P_0 H_k + P_k H_0)\, d\theta \cdot d\zeta
$$

Appendix B

(1) $\left[\frac{p_{i,j}}{pS} \le \left[\frac{2}{\kappa+1}\right]^{\kappa/\kappa-1}\right]$

$$Q_0 = \Gamma_S P_S H_0 \left[\frac{2\kappa}{\kappa+1}\right]^{1/2}\left[\frac{2}{\kappa+1}\right]^{1/\kappa-1}$$

$$Q_1 = \Gamma_S P_S H_1 \left[\frac{2\kappa}{\kappa+1}\right]^{1/2}\left[\frac{2}{\kappa+1}\right]^{1/\kappa-1}$$

$$Q_2 = \Gamma_S P_S H_2 \left[\frac{2\kappa}{\kappa+1}\right]^{1/2}\left[\frac{2}{\kappa+1}\right]^{1/\kappa-1}$$

(2) $\left[\frac{p_{i,j}}{pS} > \left[\frac{2}{\kappa+1}\right]^{\kappa/\kappa-1}\right]$

$$Q_0 = \Gamma_S P_S H_0 \left(\frac{2\kappa}{\kappa-1}\right)^{1/2}\left[\left(\frac{P_0}{P_S}\right)^{2/\kappa} - \left(\frac{P_0}{P_s}\right)^{\kappa+1/\kappa}\right]^{1/2}$$

$$Q_1 = \Gamma_S P_S \left(\frac{2\kappa}{\kappa-1}\right)^{1/2}\left[\frac{H_0\left\{\frac{2}{\kappa}\left(\frac{P_0}{P_S}\right)^{2-\kappa/\kappa}\left(\frac{P_1}{P_S}\right) - \frac{\kappa+1}{\kappa}\left(\frac{P_0}{P_S}\right)^{1/\kappa}\left(\frac{P_1}{P_S}\right)\right\}}{2\left[\left(\frac{P_0}{P_S}\right)^{2/\kappa} - \left(\frac{P_0}{P_S}\right)^{\kappa+1/\kappa}\right]^{1/2}} + H_1\left[\left(\frac{P_0}{P_S}\right)^{2/\kappa} - \left(\frac{P_0}{P_S}\right)^{\kappa+1/\kappa}\right]^{1/2}\right]$$

$$Q_2 = \Gamma_S P_S \left(\frac{2\kappa}{\kappa-1}\right)^{1/2}\left[\frac{H_0\left\{\frac{2}{\kappa}\left(\frac{P_0}{P_S}\right)^{2-\kappa/\kappa}\left(\frac{P_2}{P_S}\right) - \frac{\kappa+1}{\kappa}\left(\frac{P_0}{P_S}\right)^{1/\kappa}\left(\frac{P_2}{P_S}\right)\right\}}{2\left[\left(\frac{P_0}{P_S}\right)^{2/\kappa} - \left(\frac{P_0}{P_S}\right)^{\kappa+1/\kappa}\right]^{1/2}} + H_2\left[\left(\frac{P_0}{P_S}\right)^{2/\kappa} - \left(\frac{P_0}{P_S}\right)^{\kappa+1/\kappa}\right]^{1/2}\right]$$